Numeric Simulation of Heat Transfer and Electrokinetic Flow in an Electroosmosis-Based Continuous Flow PCR Chip

ARTICLE *in* ANALYTICAL CHEMISTRY · OCTOBER 2006

Impact Factor: 5.64 · DOI: 10.1021/ac060553d · Source: PubMed

2 AUTHORS:

Lin Gui
Technical Institute of Physics and Chemistry
18 PUBLICATIONS **131** CITATIONS

SEE PROFILE

Carolyn L Ren
University of Waterloo
68 PUBLICATIONS **2,979** CITATIONS

SEE PROFILE

Anal. Chem. **2006,** *78,* 6215−6222

Numeric Simulation of Heat Transfer and Electrokinetic Flow in an Electroosmosis-Based Continuous Flow PCR Chip

Lin Gui and Carolyn L. Ren*

Department of Mechanical Engineering, University of Waterloo, 200 University Avenue West, Waterloo, Ontario, Canada N2L 3G1

Precise design and operational control of the polymerase chain reaction process is key to the performance of on-chip DNA analysis. This research is dedicated to understanding the fluid flow and heat transfer mechanisms occurring in continuous flow PCR chips from the engineering point of view. In this work, a 3-dimensional model was developed to simulate the electrical potential field, the flow field, and the temperature field in an electroosmosis-based continuous flow PCR chip. On the basis of the simultaneous solution to this model, the effects of the channel/chip size, the chip material, and the applied voltage difference on the temperature distribution and control are discussed in detail. The importance of each heat transfer mechanism for different situations is also discussed. It was found that if a larger chip thickness or a material with a lower heat conductivity was used, the temperature in the microfluidic PCR chip would decrease dramatically. The effects of the applied electrical field strength and flow velocity on the temperature distribution, however, are negligible for microchannels with a small cross-sectional area. With bigger channels, the flow direction will affect the temperature distribution in the channel because heat convection will dominate heat transfer.

The polymerase chain reaction (PCR), which is a powerful technique used to exponentially amplify specific target DNA sequences by processing the sample repetitively through a thermal cycle, has been widely used in chemical and biomedical diagnosis and analysis.[1−3] A single thermal cycle in PCR processes generally includes three steps. In the first step, the sample is heated to ∼95 °C to let a double-stranded DNA molecule be denatured into two single-stranded DNA molecules; in the second step, the sample is cooled to ∼60 °C for annealing of the primers to the single-stranded DNA template; and finally, that is, in the third step, the temperature is raised a little to ∼75 °C for extension of the target DNA in the presence of a polymerization enzyme and deoxynucleotide triphosphates. By processing one single cycle, the amount of target DNA molecule can be theoretically amplified by 2. After repeating multiple cycles, the amount will be amplified exponentially. This technology allows a small amount of specific DNA sequence to be amplified rapidly within several hours.[4−5]

There has been interest in developing microfluidic chips for PCR applications,[6−8] because the inherent larger surface-to-volume ratio of microfluidic devices will lead to lower sample/reagent consumption and higher heat transfer efficiency, and thus, a much faster biochemical reaction speed. For example, Daniel at al.[9] developed a miniaturized silicon reaction chamber using photolithography and wet etching technologies for PCR applications. The good features of this design include small reagent volumes of ∼1 μL, low power operation, and fast processing time of ∼10 min for 30 cycles. In 1994, Nakano[10] reported continuous flow PCR experiments in which the reaction mixture was continuously pumped through a thin Teflon capillary and was treated with three successive thermal stages for denaturation, annealing, and extension. Although a capillary was used for that process instead of a serpentine channel on a chip, this is the first introduction of the continuous flow PCR concept. With the development of chip technology, continuous flow PCR chips have been developed lately. For example, Kopp presented such a microfluidic PCR chip that shortened PCR processing time significantly to as low as 90 s for 20 cycles, during which the solution mixture was pumped through three stable temperature regions repetitively.[11] The major advantage of the continuous flow PCR chip over chamber-based microfluidic PCR chips is that the time spent on conquering the thermal inertia of the apparatus can be largely saved. The total processing time, therefore, can be reduced from the original 3 h to ∼1.5 to 18.5 min for 20 cycles. Recently, Hashimoto et al.[12] also reported a continuous flow PCR chip in which spiral microchannels were used for different PCR processing steps and the reduction of reaction time was achieved by increasing flow velocity.

* Corresponding author. Phone: 519-888-4567, x 3030. Fax: 519-885-5862. E-mail: c3ren@mecheng1.uwaterloo.ca.

(1) Liao, C. S.; Lee, G. B.; Wu, J. J.; Chang, C. C.; Hsieh, T. M.; Huang, F. C.; Luo, C. H. *Biosens. Bioelectron*. **2005**, *20*, 1341−1348.
(2) Chang, H. C.; Leaw, S. N.; Huang, A. H.; Wu, T. L.; Chang, T. C. *J. Clin. Microbiol.* **2001**, *39*, 3466−3471.
(3) Brauns, T. C.; Goos, M. *J. Cutan. Pathol*. **2005**, *32*, 461−466.
(4) Chang, H. C.; Leaw, S. N.; Huang, A. H.; Wu, T. L.; Chang, T. C. *J. Clin. Microbiol.* **2001**, *39*, 3466−3471.
(5) Gillespie, S. H.; Ullman, C.; Smith, M. D.; Emery, V. *J. Clin. Microbiol.* **1994**, *32*, 1308−1311.
(6) Liu, D. Y.; Zhou X. M.; Zhong, R. T.; Ye N. N.; Cheng G. H.; Xiong, W.; Mei, X. D.; Lin, B. C. *Talanta* **2006**, *68*, 616−622.
(7) Khandurina, J.; McKnight, T. E.; Jacobson, S. C.; Waters, L. C.; Foote, R. S.; Ramsey, J. M. *Anal. Chem.* **2000**, *72*, 2995−3000.
(8) Aroux, P. A.; Koc, Y.; Mello, A.; Manz, A.; Day, P. J. R. *Lab Chip* **2004**, *4*, 534−546.
(9) Daniel, J. H. *Sens. Actuators, A* **1998**, *71*, 81−88.

10.1021/ac060553d CCC: $33.50
Published on Web 08/02/2006

However, the integration of PCR and other associated processes into a microfluidic chip platform to achieve the micro total analysis has been hindered due to the lack of systematic design and operational control of PCR processes. To this end, recently, different kinds of continuous flow PCR chips have been extensively studied. Generally speaking, there are three kinds of continuous flow PCR chips:[13] unidirectional,[10−11,14−17] closed-loop,[18−22] and oscillatory chips.[23−24] Although closed-loop and oscillatory chips have more flexibility to increase or decrease the number of thermal cycles than unidirectional chips, they also increase the complexity of fabrication. In most applications, the number of thermal cycles is not required to change; therefore, if the number of thermal cycles is optimally designed, a unidirectional chip is an ideal design for on-chip PCR analysis.

There are two commonly used methods for driving liquids through a microfluidic chip. One is pressure-driven flow, such as that employed in the design used by Kopp et al.,[11] and the other one is electrokinetic flow. Each method has its pros and cons, and electrokinetic flow is normally preferred in lab-on-a-chip applications due to its flat and plug-like velocity profile reducing sample dispersion and the degree of flowrate control it allows.[25−26] Furthermore, if using electrokinetic flow, no moving element is required in the system, and electric control makes the system very easy to operate and integrate expediently. Electrokinetic flow has not been widely used in PCR applications so far, due to the need of the high voltage for pumping liquid. Therefore, considering the merits that electrokinetic flow can offer, this paper is aimed at exploring the possibility of employing electrokinetic flow for a unidirectional PCR chip design through investigation of the effects of multiple controlling parameters, such as the layout of microchannels, channel geometry, applied electrical field strength, or chip material on PCR processes.

To propose an optimized configuration for a continuous flow PCR chip, it is essential to gain a thorough understanding of fluid flow and heat transfer in such a microfluidic chip, where heat transfer occurs in both the solid and liquid regions. Numerical simulation has been proved to be an excellent alternative to experimental studies for rapid prototyping of labs-on-a-chip,[27] since it allows extensive parametric studies within a short time period. Therefore, this report will focus on numerical studies of fluid flow and heat transfer in a microfluidic chip for PCR applications.

The numerical studies of heat transfer and fluid flow in microfluidic chips[28−34] are too numerous to be listed here. A few studies about thermal simulation of a chamber-based PCR chip[28−30] have been reported; however, there are few numerical studies about continuous flow PCR chips. Recently, Zhang et al.[31] presented both numerical and experimental studies about a continuous flow PCR chip in which the commercial software ANSYS was used to obtain the temperature field in the entire chip. Their experimental results agree well with their numerical predictions. In their simulation, they did not consider the influences of the channel dimension and the liquid convection on heat transfer in the PCR chip. To systematically design and operationally control on-chip PCR processes, it is essential to develop a 3-D numerical model to simulate the electrical potential field, flow field, and thermal field prior to chip fabrication and characterization. In the following sections, the physical model, mathematical model, results, and discussions are provided in detail.

MATHEMATICAL MODEL

Computational Module. Figure 1 shows a sketch of the microchannel layout in a continuous flow PCR chip proposed and studied in this paper. The whole chip is divided into three regions, with different temperatures along the x direction. A long, wandering microchannel is proposed; however, for the convenience of model development, a single repetitive element appearing in the entire chip is chosen as the computational module. Considering the periodical property, the whole channel can be segmented into many U-shaped channels, as shown in Figure 1b. Both the electrical potential field and the flow field simulation can be performed first in an upper U-shaped computation module and then mapped into the lower U-shaped modules, which allows the electrical potential and flow fields for the entire channel to be completed by connecting the upper and lower U-shaped modules alternately. However, for the temperature field, the upper U-shape module cannot be simply mapped into the lower module because of the existence of natural convection. Instead, both the upper module and the lower module should be considered as a single computation module for the thermal field simulation, as shown in Figure 1c, which has a dimension of $L = 6.4$ cm and $W = 4.1$ mm. The typical chip thickness is chosen as $H = 2$ mm. These dimensions will be used in most simulations in the following,

(10) Nakano, H.; Matsuda, K.; Yohda, M.; Nagamune, T.; Endo, I.; Yamane, T. *Biosci. Biotechnol. Biochem.* **1994**, *58*, 349−352.
(11) Kopp, M. U.; Mello, A. J.; Manz, A. *Science* **1998**, *280*, 1046−1048.
(12) Hashimoto, M.; Chen, P. C.; Mitchell, M. W.; Nikitopoulos, D. E.; Soper, S. A.; Murphy, M. C. *Lab Chip* **2004**, *4*, 638−645.
(13) Chen, Z. Y.; Qian, S. Z.; Abrams, W. R.; Malamud, D.; Bau, H. H. *Anal. Chem.* **2004**, *76*, 3707−3715.
(14) Obeid, P. J.; Christopoulos, T. K.; Crabtree, H. J.; Backhouse, C. J. *Anal. Chem.* **2003**, *75*, 288−295.
(15) Sun, K.; Yamaguchi, A.; Ishida, Y.; Matsuo, S.; Misawa, H. *Sens. Actuators, B* **2002**, *84*, 283−289.
(16) Curcio, M.; Roeraade, J. *Anal. Chem.* **2003**, *75*, 1−7.
(17) Park, N.; Kim, S.; Hahn, J. H. *Anal. Chem.* **2003**, *75*, 6029−6033.
(18) Liu, J.; Enzelberger, M.; Quake, S. *Electrophoresis* **2002**, *23*, 1531−1536.
(19) Chou, C. F.; Changrani, R.; Roberts, P.; Sadler, D.; Burdon, J.; Zenhausern, F.; Lin, S.; Mulholland, A.; Swami, N.; Terbrueggen, R. *Microelectron. Eng.* **2002**, *61−62*, 921−925.
(20) Bau, H. H. *IMECE 2001, MEMS 23884 Symposium Proceedings*, New York, November, 2001.
(21) Bau, H. H.; Zhu, J.; Qian, S.; Xiang, Y. *Sens. Actuators, B* **2003**, *88*, 205−216.
(22) West, J.; Karamata, B.; Lillis, B.; Gleeson, J. P.; Alderman, J.; Collins, J. K.; Lane, W.; Mathewson, A.; Berney, H. *Lab Chip* **2002**, *2*, 224−230.
(23) Bu, M. Q.; Tracy, M.; Ensell, G.; Wilkinson, J. S.; Evans, A. G. R. *J. Micromech. Microeng.* **2003**, *13*, S125−S130.
(24) Wang, W.; Li, Z. X.; Luo, R.; Lv, S. H.; Xu, A. D.; Yang, Y. J. *J. Micromech. Microeng.* **2005**, *15*, 1369−1377.
(25) Ross, D.; Johnson, T. J.; Locascio, L. E. *Anal. Chem.* **2001**, *73*, 2509−2515.
(26) Sinton, D.; Erickson, D.; Li, D. *J. Micromech. Microeng.* **2002**, *12*, 898−904.
(27) Erickson, D. *Microfluid. Nanofluid.* **2005**, *1*, 301−318.
(28) Yan, W. P.; Du, L. Q.; Wang, J.; Ma, L. Z.; Zhu, J. B. *Sens. Actuators, B* **2005**, *108*, 695−699.
(29) El-Ali, J.; Perch-Nielsen, I. R.; Poulsen, C. R.; Bang, D. D.; Telleman, P.; Wolff, A. *Sens. Actuators,* A **2004**, *110*, 3−10.
(30) Lin, Y. C.; Yang, C. C.; Huang, M. Y. *Sens. Actuators, B* **2000**, *71*, 127−133.
(31) Zhang, Q. T.; Wang, W. H.; Zhang, H. S.; Wang, Y. L. *Sens. Actuators, B* **2002**, *82*, 75−81.
(32) Patankar, N. A.; Hu, H. H. *Anal. Chem.* **1998**, *70*, 1870−1881.
(33) Fu, L. M.; Yang, R. J.; Lee, G. B.; Liu, H. H. *Anal. Chem.* **2002**, *74*, 5084−5091.
(34) Lammertink, R. G. H.; Schlautmann, S.; Besselink, G. A. J.; Schasfoort, R. B. M. *Anal. Chem.* **2004**, *76*, 3018−3022.

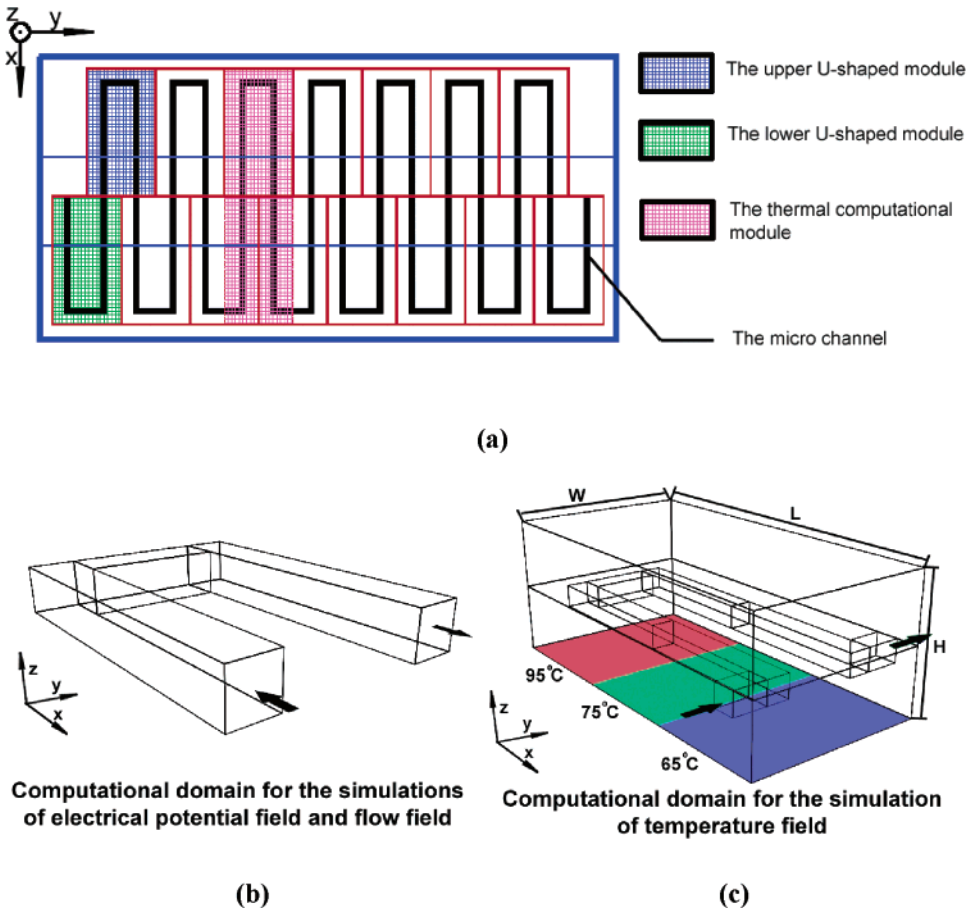

Figure 1. Sketch of computational modules (not drawn to scale).

unless stated otherwise. Although the layout of the channel does not fully consider the processing time ratio among the three phases, it is sufficient to reveal the mechanism of flow and heat transfer in a microfluidic chip to a certain extent. In numerical simulations, it is assumed that the chip consists of three layers: the upper layer, the middle layer with microchannels, and the lower layer. Both the middle and the lower layers constitute the lower substrate mentioned before.

Electrical Potential Field. To drive a liquid through a microchannel by an electroosmotic pump, a certain electrical potential difference must be applied between the two ends of the microchannel. Considering a uniform buffer concentration and ignoring net charges in the bulk liquid, which is reasonable for most PCR applications in which the electrical double layer thickness is extremely small as compared to the channel dimension, one can write the nondimensional governing equation for the electrical potential field in the U-shaped module as

$$\nabla^2\Phi = 0 \tag{1}$$

where $\Phi = \psi/V_0$ is the nondimensional electrical potential, and V_0 is the electrical potential difference applied between the two ends of the U-shaped module. Considering the substrate is made of insulation materials, the insulation boundary condition $\partial\Phi/\partial n|_{wall} = 0$ is applied to all the channel walls. The specific voltages are applied to the two ends of the U-shaped module, such as $\Phi|_{inlet} = \Phi_{applied}$.

Flow Field. Compared to the typical channel dimensions for most PCR applications, the thickness of the electrical double layer (EDL) is very small. For example, the concentration of commonly used buffer solutions in PCR applications is on the order of millimolar, which gives rise to a double layer thickness of <10 nm. Therefore, the EDL can be treated as a superthin layer near the wall, where net charges only exist. Under this consideration, electroosmotic flow in a microchannel can be simply treated as a "boundary-driven" flow. In this simplified "boundary-driven" flow, no electric body force item exists in the momentum equation, and a slip boundary condition is applied, instead, which has been used successfully before.[35] Thus, the nondimensional governing equations can be written as

$$Re\left[\frac{\partial\vec{U}}{\partial\tau} + (\vec{U}\cdot\vec{\nabla})\vec{U}\right] = -\vec{\nabla}P + \nabla^2\vec{U} \tag{2}$$

where $\vec{U}$ is the nondimensional velocity ($\vec{U} = \vec{u}/U_0$, where U_0 is the mean inlet velocity), Re is the Reynolds number ($Re = U_0 l/\nu$ where l is the characteristic length taken to be the width of the channel here and ν is the kinematic viscosity of the fluid), τ is the nondimensional time ($\tau = t/t_0$ where $t_0 = l/U_0$ is the characteristic time), and P is the nondimensional pressure ($P = p/(\mu U_0/l)$, where μ is the dynamic viscosity of the fluid). In general, t_0 is very small (i.e., on the order of microseconds)

(35) Hu, Y. D.; Werner, C.; Li, D. Q. *Anal. Chem.* **2003**, *75*, 5747−5758.

because l is on the order of micrometers, and U_0 is on the order of millimeters per second. That is to say that the flow field should attain equilibrium in several milliseconds. For simplicity, the transient term in eq 2 can be ignored safely, and the final governing equation is reduced to

$$\mathrm{Re}(\vec{U}\cdot\vec{\nabla})\vec{U} = -\vec{\nabla}P + \nabla^2\vec{U} \tag{3}$$

and the continuity equation is

$$\vec{\nabla}\cdot\vec{U} = 0 \tag{4}$$

Considering the length of the channel is much longer than the width, the zero-flux boundary condition is applied to the inlet and outlet of the U-shaped module ($\partial\vec{U}/\partial n|_{\mathrm{inlet}} = 0, \partial\vec{U}/\partial n|_{\mathrm{outlet}} = 0$). The slip boundary condition is used at the wall surface such as $\vec{U}|_{\mathrm{wall}} = \mu_{\mathrm{eo}}\vec{E}/U_0$, where $\vec{E} = -\nabla\vec{\psi}$ is the applied electric field intensity and μ_{eo} is the electroosmotic mobility of the fluid.

Thermal Field. Heat transfer occurs cross the entire chip, including both the solid substrates and the liquid regions. During the simulation, all the fluid and substrates are considered as one material with variable thermal properties. Because PCR processes often begin after the thermal field of the whole PCR chip already attains equilibrium, the characteristic length is still the width of the microchannel. Thus, the nondimensional governing equation can be given as follows

$$\bar{\rho}C_{\mathrm{p}}\left[\frac{\partial\Theta}{\partial\tau} + Pe\vec{U}\cdot\vec{\nabla}\Theta\right] = \vec{\nabla}(\Lambda\cdot\vec{\nabla}\Theta) + \dot{Q} \tag{5}$$

where $\bar{\rho}$ is the nondimensional density ($\bar{\rho} = \rho/\rho_0$, where ρ_0 is the density of the solution), C_{p} is the nondimensional heat capacity ($C_{\mathrm{p}} = c/c_0$, where c_0 is the heat capacity of the solution), Λ is the nondimensional heat conductivity ($\Lambda = \lambda/\lambda_0$, where λ_0 is the heat conductivity of the solution), Θ is the nondimensional temperature ($\Theta = (T - T_{\mathrm{low}})/(T_{\mathrm{high}} - T_{\mathrm{low}})$ where $T_{\mathrm{high}} = 95$ °C is taken to be the temperature of denaturation, and $T_{\mathrm{low}} = 65$ °C, the temperature of annealing), $\dot{Q}$ is the nondimensional heat resource ($\dot{Q} = \dot{q}l^2/\lambda_0(T_{\mathrm{high}} - T_{\mathrm{low}})$), Pe is the Peclet number ($Pe = U_0l/\alpha_0$ where α_0 is the thermal diffusivity of the solution), and τ is the nondimensional time ($\tau = t/t_1$, where $t_1 = l^2/\alpha_0$ is the characteristic time of heat transfer in microchannels). What should be pointed out here is that the velocity of nonliquid materials should be considered as zero during the simulation. In general, the characteristic time t_1 is very small (i.e., 0.015 s) when considering that the characteristic length l is 50 μm and $\alpha_0 = 16.9 \times 10^{-8}$ m^2/s. That is to say that the thermal field will attain equilibrium within 0.02 s, so it is safe to ignore the transient item in eq 5 again.

$$\bar{\rho}C_{\mathrm{p}}Pe\vec{U}\vec{\nabla}\Theta = (\Lambda\vec{\nabla}\Theta) + \dot{Q} \tag{6}$$

Constant temperature distribution is used as the boundary condition at the bottom surface of the chip to simulate the three temperature zones (95, 75, and 65 °C), as discussed above. Figure 1c shows the bottom temperature distribution. Natural convection is considered as the boundary condition of the top surface,

$$\frac{\lambda_0}{l}\Lambda\left.\frac{\partial\Theta}{\partial Z}\right|_{\mathrm{top}} = \hbar_\infty(\Theta_{\mathrm{wall}} - \Theta_\infty) \tag{7}$$

where, $\hbar_\infty$ is the heat transfer coefficient of natural convection, Θ_∞ is the nondimensional room temperature ($\Theta_\infty = (T_\infty - T_{\mathrm{low}})/(T_{\mathrm{high}} - T_{\mathrm{low}})$, where $T_\infty = 25$ °C is chosen here), and Θ_{wall} is the nondimensional temperature at the top surface. $\hbar_\infty$ is given by

$$\hbar_\infty = Nu\frac{\lambda_{\mathrm{air}}}{L} \tag{8}$$

where, λ_{air} is the air heat conductivity, L is the chip length, and Nu is the Nussel number of natural convection that is chosen from[36]

$$Nu = 0.62(GrPr)^{0.25} \tag{9}$$

where Gr is the Grashof number ($Gr = g\beta\Delta TL^3/\upsilon_{\mathrm{air}}^2$ where g is the gravitational acceleration; β is the thermal expansion coefficient, which for gases is $1/T$; ΔT is the temperature difference between the wall and ambient air; υ_{air} is the kinematic viscosity of air); and Pr is the Prandtl number of air.

Because all the modules should be connected in the end to show the thermal field of the entire chip, periodic boundary conditions are used at the two side sectional faces ($y = 0$ and $y = W$). Compared with the chip length, chip thickness is very small, (for example, $H/L = 2$ mm/6 cm = 3.3%); therefore, the natural convection at such a small surface can be neglected compared to the natural convection at the top surface. Under this consideration, an adiabatic boundary condition is adopted in the simulation at $x = 0$ and $x = L$.

RESULTS AND DISCUSSIONS

The 3D model was solved using a specially developed program written in the C^{++}-based finite control volume method. In the following parametric studies, without losing generality, most physical and thermal properties of the liquid were chosen from that of pure water, considering the concentration of most commonly used buffer solutions in PCR applications is on the order of millimolar. Two kinds of ordinary solid materials, glass and PDMS, were considered for PCR chip materials. The detailed running parameters used here are listed in Table 1.[37]

Analytical Validation of Computational Model. To validate the developed numerical model, a comparison between the analytical and numerical solutions of the temperature field was performed along the chip thickness direction at the center of the high-temperature zone of 95 °C. The justification of the comparison is provided below. When the channel is very thin (50 μm × 50 μm in cross-sectional area), the impact of the channel dimension on the temperature field of the entire chip is negligible because the total heat capacity of the channel is <0.01% that of the entire chip. Generally, the chip thickness, H, is very small, as compared

(36) Yousef, W. W.; Tarasuk, J. D.; McKenn, W. J. *J. Heat Transfer* **1982**, *104*, 493−500.

(37) Ren, L. Q.; Sinton, D.; Li, D. Q. *J. Micromech. Microengin.* **2003**, *13*, 739−747.

Table 1. Typical Running Parameters

	λ (W/m K)	ρ (kg/m^3)	c (J/kg °C)	υ (m^2/s)		
water	0.684	1.05×10^3	4180		g	9.8 m/s^2
glass	1.1	2.2×10^3	700		Pr	0.698
PDMS	0.15	0.97×10^3	1460		$\mu_{\epsilon 0}$[42]	4.5×10^{-8} m^2/V s
air	2.83×10^{-2}			1.795×10^{-5}		

with the chip length; therefore, the heat transfer along the *x*- or *y*-direction (the length or width direction) should be relatively weak, as compared with the *z*-direction (the thickness direction). This means that the temperature distribution along the *z*-direction at the center of the temperature zones should be very similar to that obtained using the heat transfer model of infinite multilayer planes.

Assume that there are two infinite planes in an environment of air. The bottom temperature of the lower layer is constant at T_0. With the theory of heat resistance, the temperature distribution along the *z*-direction can be obtained easily,

$$T = \begin{cases} T_0 - \dfrac{(T_0 - T_f)}{\delta_1/\lambda_1 + \delta_2/\lambda_2 + 1/\alpha} \cdot \dfrac{z}{\lambda_1} & 0 < z \le \delta_1 \\ T_0 - \dfrac{(T_0 - T_f)}{\delta_1/\lambda_1 + \delta_2/\lambda_2 + 1/\alpha}\left(\dfrac{\delta_1}{\lambda_1} + \dfrac{z - \delta_1}{\lambda_2}\right) & \delta_1 < z \le \delta_1 + \delta_2 \end{cases} \quad (10)$$

where T_f is the ambient temperature, δ_1 and λ_1 are the thickness of the lower layer and its heat conductivity, δ_2 and λ_2 are the thickness of the upper layer and its heat conductivity, and α is the heat transfer coefficient of natural convection.

As shown in Figure 2, the numerical solution of the temperature along the *z*-direction at the center of the channel agrees perfectly with the analytical solution. This validates the developed numerical model, which was used to perform the parametric studies reported below.

Temperature Field. To reveal the thermal behavior of the entire chip, which has significant effects on the PCR chip performance, parametric studies of heat transfer in the entire chip were performed.

Effects of Chip Material. Because different materials have quite different thermal properties, which will affect temperature ramping between different temperature zones, chip material is surely the most important factor to be considered in PCR chip design. Two kinds of commonly used materials, glass and PDMS, are considered here. Figures3 and 4 show the influence of the chip material on the temperature distribution. Figure 3 shows the temperature distributions at the middle horizontal plane (containing the liquid region) of a PDMS chip and at the two vertical planes standing right on the two arms of the U-shaped module. Two subfigures shown at the left and right bottom corners clearly indicate the three temperature zones achieved in the left and right arms, respectively. Please note that for PCR applications, a longer channel length should be designed for the extension region (i.e., temperature is 75 °C), allowing sufficient time for extension. However, the purpose of this study is to develop a 3-D numerical model allowing us to perform parametric studies of heat transfer

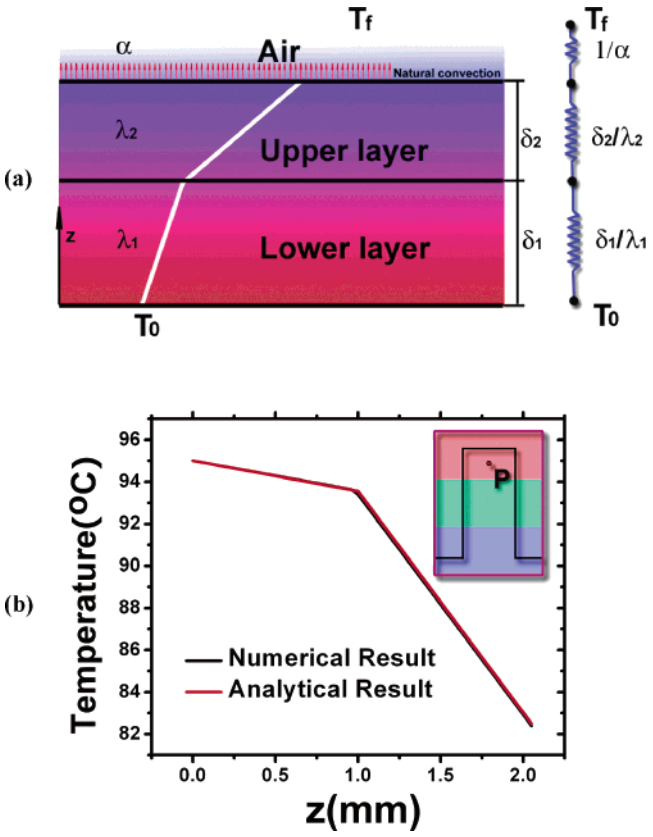

Figure 2. (a) Sketch of the analytical model for multilayer heat transfer and (b) comparison between numerical and analytical results of the temperature at point P.

and fluid flow in an electrokinetic flow-based continuous flow PCR chip. Therefore, this feature is not considered for most cases. However, on the basis of the investigations performed here, this feature was eventually considered in a potential design proposed by the developed model, which will be discussed at the end of this paper.

Figure 4 shows the temperature field distribution at the middle horizontal plane of a hybrid glass/PDMS chip. One can see that because the heat conductivity of glass (i.e. 1.1 W/mK) is much higher than that of PDMS (i.e. 0.15 W/m*K*), and thus, heat transfer occurs more efficiently cross the lower glass substrate, which reduces the temperature variation along the *z*-direction. For this specific application, the largest temperature drop from the bottom plate, where a constant temperature field for three regions is assumed, to the middle plane of the chip is only 1.85 °C. This can be further observed from the temperature distribution of the left and right arms shown in the subfigures. The chip made completely of glass has also been studied, and it was found that the largest temperature drop is only 1.76 °C from the bottom surface to the middle horizontal plane, where the microchannel

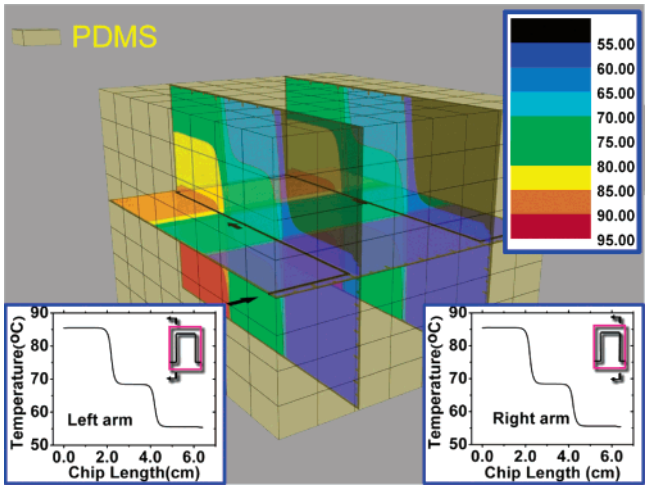

Figure 3. Temperature field of a PDMS chip with a height of 2.0 mm.

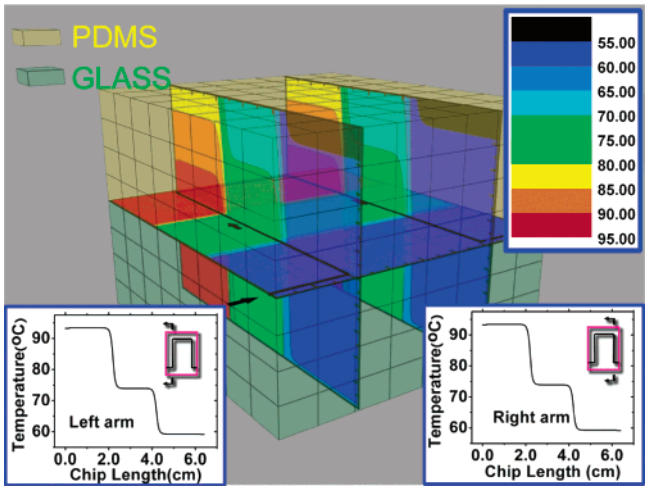

Figure 4. Temperature field of a hybrid PDMS/glass chip with a height of 2.0 mm.

exists (figure is not shown). Comparing these three designs, a glass chip is an ideal choice in terms of temperature control; however, a hybrid PDMS/glass chip is also an acceptable design for PCR applications.

Effects of Chip Thickness. Because the main heat transfer direction in the proposed design is from bottom to top, another key parameter that might greatly affect the temperature field is chip thickness. Figure 5 shows the temperature field in a hybrid PDMS/glass chip with a thickness of 4 mm, which is double the thickness considered in Figure 4. It can be seen that the thicker the chip, the lower the fluid temperature. This is because the temperature drops more from the bottom to the middle horizontal plane when substrates become thicker. For example, the temperature drops about 2.8 °C in Figure 5 and only 1.76 °C in Figure 4 cross the same thickness, which results in a lower liquid temperature in Figure 5 (1 °C lower than that in Figure 4) due to its larger material thickness.

Effects of Channel Cross-Sectional Area. To see the influence brought by channel cross-sectional area, two channel sizes, 50 μm × 50 μm and 500 μm × 500 μm, were studied. Figure 6 shows the temperature field for different channel sizes with the same chip materials (PDMS, upper layer, and glass, lower layer). The

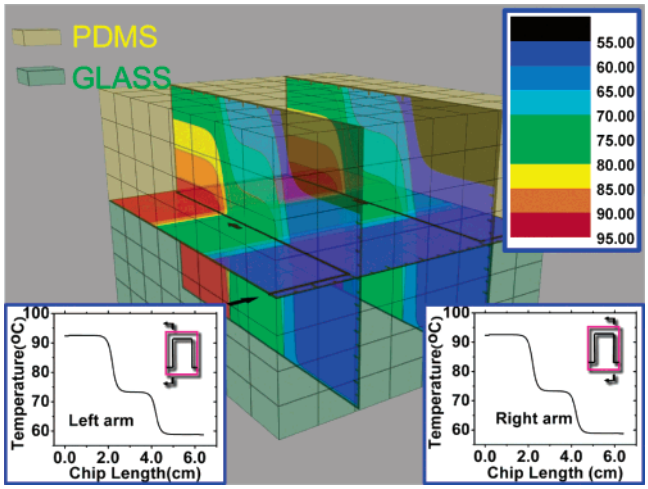

Figure 5. Temperature field of a hybrid PDMS/glass chip with a height of 4.0 mm.

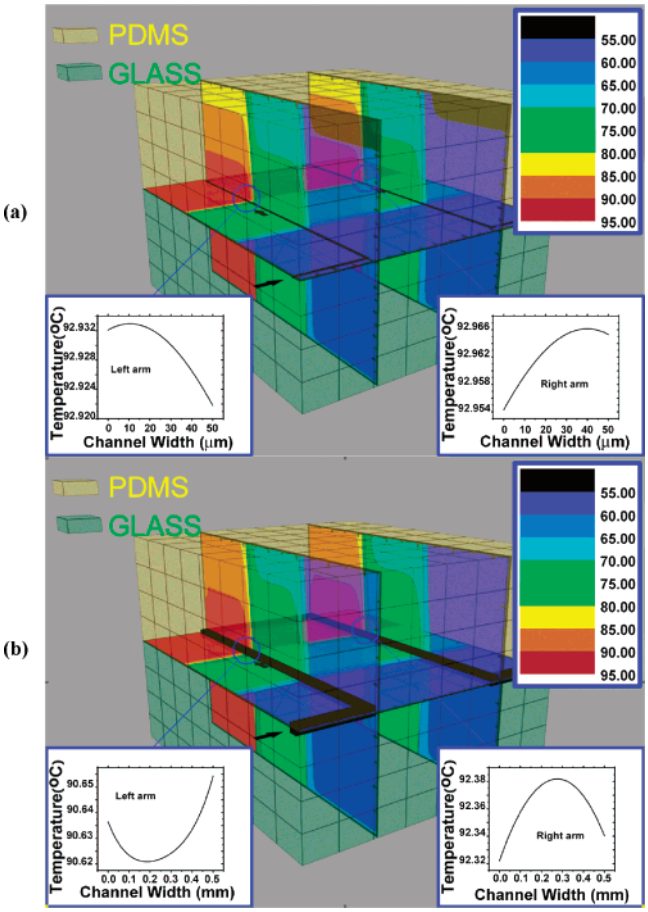

Figure 6. Temperature field of a hybrid PDMS/glass chip with different channel sizes, (a) 50 μm × 50 μm and (b) 500 μm × 500 μm.

subfigures show the temperature variation of the fluid across the channel width at the interface between the high/medium temperature regions. The total temperature change cross the channel width is small for both scenarios; however, it is worth noticing that the temperature variation trends of the two arms are quite different between the two situations, which are due to different primary heat transfer mechanisms and can be understood as follows.

There are two major heat transfer mechanisms in the channel: heat conduction and heat convection. Heat conduction is determined by the heat conductivity of the medium, and heat convection is determined by the heat capacity and momentum transfer of the fluid. If channel size is very small, say 50 μm × 50 μm, as shown in Figure 6a, the momentum heat transfer of the fluid is negligible because of its low heat capacity as compared with that of the entire chip (<0.003% of the entire chip). Therefore, heat conduction dominates heat transfer in the microchannel. As shown in Figure 6a, the velocity of the fluid has little impact on the temperature field. That is the reason the temperature trends of the left and right arms showed in the subfigures of Figure 6a are still the same, although the flow direction is different. This has also been assumed by Zhang et al.[31] in their chip design using numerical analysis tools, and their design was validated by their experimental results. The temperature at the center of the channel width is higher than that at both side walls because the heat conductivity of the fluid is smaller than that of the glass.

As one can see, the temperature distribution for the bigger channel size is quite different, as shown in Figure 6b. Because the channel size is much larger, on the contrary, heat convection dominates heat transfer in the microchannel. Because of the opposite flow directions in the left and right arms, the temperature trends showed in the subfigures of Figure 6b are also opposite. In the left arm, the fluid flows from the low-temperature region to the high-temperature region, and the center of the channel is then cooled by the cooler fluid coming from the low-temperature region. Therefore, the temperature in the middle is lower than both sides in the left arm, and vice versa. Because heat conduction still exists and it tends to increase the temperature at the center of the channel, the temperature difference between the center and the side walls is much smaller in the left arm (~0.035 °C) than in the right arm (~0.06 °C).

Effects of Applied Electrical Field Strength. Influence of the applied electrical field strength was also studied. Compared with those of the material, thickness, and channel size, the influence of the applied electrical field is relatively small. A simulation with an applied voltage of 200 V shows a maximum temperature difference of only 0.21 °C with a small-channel chip of 50 μm × 50 μm and 3.2 °C for a large-channel chip of 500 μm × 500 μm (figure is not shown).

Application of the Developed Model to a Real PCR Chip Design. As discussed above, when the microchannel cross-sectional area is small, liquid convection, which depends on the applied electrical field strength and liquid properties, has little effect on the temperature distribution. Therefore, when designing a microfluidic PCR chip with a small cross-sectional area (i.e., 50 μm × 50 μm), the temperature field can be obtained by neglecting the existence of the liquid region, which simplifies the numerical analysis significantly and allows a proper design to be proposed quickly. This has been successfully applied to the studies by Zhang et al.[31] Figure 7a proposes a design for a PCR chip using the developed model without considering the liquid region. This design considered a channel length ratio of 1:1:4 for three PCR processing steps (denaturation/annealing/extension). The chip is assumed to be made of glass for the lower layer and PDMS for the upper layer. Figure 7b shows the temperature distribution along the channel

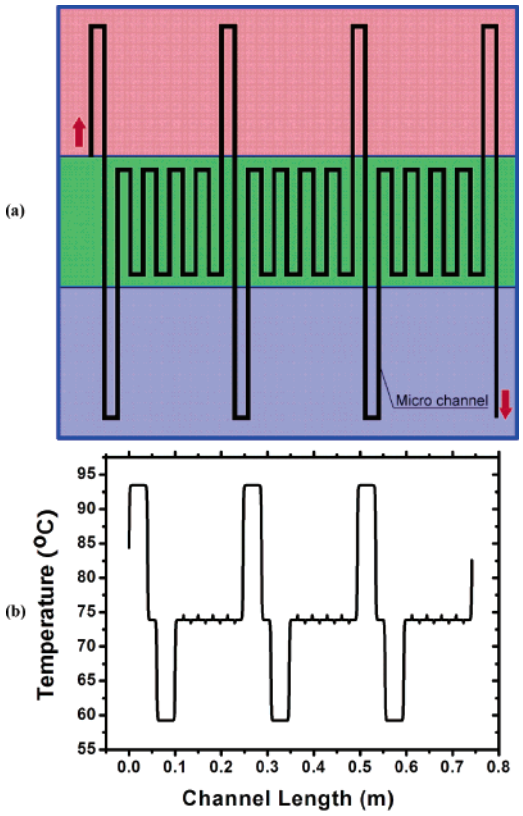

Figure 7. Proposed PCR chip. (a) Sketch of the microchannel design and (b) temperature distribution along the channel.

length obtained using the developed model. The temperature field is similar to that shown in Figure 4 except that the temperature variation along the channel length is sharper, which is ideal for PCR processes. It should be pointed out that when the channel size is bigger, neglecting the liquid region will bring more errors.

CONCLUDING REMARKS

A 3-D theoretical model was specially developed to simulate the electrical potential field, flow field and thermal field of an electrokinetic flow-based continuous flow PCR chip. It is found that chip material and chip thickness affect the thermal field greatly, regardless of the channel cross-sectional size. Because the main direction of heat transfer is from bottom to top, the material of the lower substrate is especially important for the PCR chip. When comparing PDMS and glass, the latter is recommended for the lower substrate because of its relatively high heat conductivity and low heat loss. A thinner chip thickness will also make the control of the PCR chip much easier because a much smaller temperature difference occurs between the liquid region and the bottom. When the channel cross-sectional area is small, say 50 μm × 50 μm, liquid convection has little effect on the temperature distribution because heat conduction is the primary heat transfer mechanism. Therefore, it is reasonable to design a PCR chip without considering the influences of liquid convection if the channel dimension is small. However, this approximation is not suggested for bigger channels.

From the analysis given above, it is also known that electrokinetic flow has merits as well as drawbacks. If using electrokinetic flow, no moving element is required in the system, and electric control makes the system very easy to operate and to integrate

expediently. However, unlike pressure-driven flow, if using electrokinetic flow, sample purity is another problem people should pay special attention to, because adsorption of proteins and other impurities will perturb the ζ potential and modify electroosmotic flow. Further calculation also indicates that the velocity of electrokinetic flow is relatively slow, ascompared with that of pressure-driven flow. This makes the processing time longer, although the processing time can be shortened by increasing the applied voltage or decreasing the channel length.

ACKNOWLEDGMENT

The authors gratefully acknowledge the support of a Research Grant of the Natural Sciences and Engineering Research Council (NSERC) of Canada to C. L. Ren.

Received for review March 27, 2006. Accepted June 30, 2006.

AC060553D